Solar Energy
And Sustainable Development
Refereed, biannual scientific journal issued by:
The Libyan Center for Solar Energy Research and Studies

Performance Enhancement of Microgrid Systems Using Backstepping Control for Grid Side Converter and MPPT Optimization

Mustafa Ahmad Aslan[1], Benameur Afif [2*], Mohamed Salmi[3], Boualem Merabet[4], Mohammed Berka[5], Salah Amhimmid Masoud[6].

[1]Depart. of Electrical Drives, Faculty of Electrical and Electronic Engineering, University of Aleppo, Syria.
[2,5]Faculty of Science and Technology, University Mustapha Stambouli of Mascara 29000, Algeria.
[3]Department of Physics, University of M'sila, M'sila, Algeria.
[4]Institute of Electrical Engineering, Salhi Ahmed University Center, Naama, Algeria.
[6]Zawia University, Faculty of Science, Al-Ajailat, Libya.

E-*mail:* [1] dr.mustapha.asslan@alepuniv.edu.sy ,[2] b.afif@univ-mascara.dz ,[3] mohamed.salmi@univ-msila.dz ,[4] merabet.boualem@cuniv-naama.dz ,[5] m.barka@univ-mascara.dz ,[6] s. masoud@zu.edu.ly .

ARTICLE INFO.

Article history:
Received 13 Sep 2024
Received in revised form 17 Sep 2024
Accepted 26 Nov 2024
Available online 7 Dec 2024

KEYWORDS

Backstepping controller; Microgrid Performance; Photovoltaic (PV) systems; Total Harmonic Distortion (THD); Voltage Oriented Control (VOC).

ABSTRACT

Microgrid networks represent a crucial model in the field of power transmission and distribution, integrating renewable energy sources with modern control technologies. This research focuses on enhancing the performance of a microgrid system connected to the main grid through a three-phase converter controlled using Voltage Oriented Control (VOC). The microgrid comprises a storage element and a photovoltaic (PV) generation system. To improve system efficiency and power quality, backstepping (BS) controllers are implemented and compared with traditional control methods.

Three control systems are evaluated: a conventional system using Perturb and Observe (P&O) algorithm for Maximum Power Point Tracking (MPPT) and Proportional-Integral (PI) controllers for grid-side converter (GSC) control, a hybrid system with BS-modified P&O (BS-P&O) for MPPT and PI controllers for GSC, and an advanced system employing BS-P&O for MPPT and BS controllers for GSC. The research demonstrates that BS controllers exhibit superior dynamic performance, contributing to improved regulation of DC-link voltage, active and reactive powers. Additionally, they achieve lower Total Harmonic Distortion (THD) values and increase the overall efficiency of the PV system. The proposed advanced control strategy shows particular effectiveness in tracking speed, disturbance rejection, and power quality enhancement. This study underscores the potential of nonlinear control techniques in optimizing microgrid operations and facilitating the integration of renewable energy sources into the main grid.

*Corresponding author.

DOI: https://doi.org/10.51646/jsesd.v14i1.367

تعزيز الأداء لأنظمة الشبكات المصغرة باستخدام التحكم في الخطوة الخلفية لمحول جانب الشبكة وتحسين تتبع أقصى نقطة طاقة

مصطفى أحمد أصلان، بن عامر عفيف، محمد سالمي،بوعلام مرابط ، محمد بركة، صلاح امحميد مسعود.

ملخص: تمثل الشبكات الصغيرة نموذجًا بالغ الأهمية في مجال نقل وتوزيع الطاقة، حيث تدمج مصادر الطاقة المتجددة مع تقنيات التحكم الحديثة. يركز هذا البحث على تحسين أداء نظام الشبكة الصغيرة المتصل بالشبكة الرئيسية من خلال محول ثلاثي الطور يتم التحكم فيه باستخدام التحكم الموجه بالجهد (VOC). تتكون الشبكة الصغيرة من عنصر تخزين ونظام توليد كهروضوئي (PV). لتحسين كفاءة النظام وجودة الطاقة، يتم تنفيذ وحدات تحكم خطوة خلفية (BS) ومقارنتها بطرق التحكم التقليدية. يتم تقييم ثلاثة أنظمة تحكم: نظام تقليدي يستخدم خوارزمية الاضطراب والمراقبة (P&O) لتتبع نقطة القدرة القصوى (MPPT) ووحدات تحكم التناسب التكاملي (PI) للتحكم في محول جانب الشبكة (GSC)، ونظام هجين مع P&O معدل بواسطة BS (BS-P&O) لوحدات تحكم MPPT وPI لـ GSC، ونظام متقدم يستخدم BS-P&O لوحدات تحكم MPPT وBS لـ GSC. يُظهر البحث أن وحدات التحكم في محطة القاعدة تُظهر أداءً ديناميكيًا متفوقًا، مما يساهم في تحسين تنظيم جهد وصلة التيار المستمر والقوى النشطة والتفاعلية. بالإضافة إلى ذلك، فإنها تحقق قيم تشوه توافقي إجمالي أقل وتزيد من الكفاءة الإجمالية لنظام الطاقة الكهروضوئية. تُظهر استراتيجية التحكم المتقدمة المقترحة فعالية خاصة في تتبع السرعة ورفض الاضطرابات وتحسين جودة الطاقة. تؤكد هذه الدراسة على إمكانات تقنيات التحكم غير الخطية في تحسين عمليات الشبكة الصغيرة وتسهيل دمج مصادر الطاقة المتجددة في الشبكة الرئيسية.

الكلمات المفتاحية – وحدة التحكم في الخطوة الخلفية، أداء الشبكات الصغيرة، الأنظمة الكهروضوئية، التشويه التوافقي الكلي، التحكم الموجهة للجهد.

1. INTRODUCTION

The global energy landscape is undergoing a significant transformation, driven by the imperative to reduce carbon emissions and the increasing viability of renewable energy sources. Microgrids (MGs) have emerged as a crucial model in this evolving scenario, offering a flexible and efficient approach to power transmission and distribution. These systems integrate renewable energy sources with modern control technologies, providing a bridge between traditional grid infrastructure and the decentralized, sustainable energy future. Microgrids come in two primary varieties: alternating current (AC) and direct current (DC), each offering benefits such as low losses, high reliability, and ease of installation. The growing interest in Microgrids and distributed generation (DG) systems is further fueled by recent developments in energy storage technologies and power electronics, opening new possibilities for integrating renewable energy sources with both household and industrial loads, as well as with the main electrical grid [1, 2]. MGs come in two varieties: alternating current (ACMGs) and direct current (DCMGs). All of them have the same benefits, which include low losses, versatility, high dependability, and simplicity of installation. Notably, the ease of construction of DCMGs has led to their widespread acceptance [3, 4].MGs include different types of RES such as fuel cells, geothermal, photovoltaic (PV) and wind systems [5, 6].

Among the various renewable energy sources integrated into Microgrids, photovoltaic (PV) systems have gained significant traction due to their reliability, scalability, and decreasing costs. PV panels represent a modern technology that efficiently converts solar energy into clean, renewable electrical energy, helping to reduce dependency on fossil fuels and minimize harmful emissions. The integration of PV systems into Microgrids contributes to improving the quality of life in areas where traditional electricity access is limited, while also offering long-term economic benefits through reduced energy costs and increased system efficiency [7-9]. However, the increased penetration of renewable energy sources into distribution networks presents challenges, including voltage fluctuations due to changing climatic conditions [10] and increased harmonic content resulting from the use of power electronic interfaces. Backstepping (BS) control

offers innovative solutions to the challenges faced by renewable energy sources in distribution networks. The voltage fluctuations and harmonic distortions typical in renewable energy systems can be effectively mitigated through BS's adaptive control mechanism, which provides robust stability and precise power regulation. Specifically, for PV panels with their low energy conversion efficiency (12-25%) and high initial costs, backstepping enables more dynamic maximum power point tracking, compensating for suboptimal power output by dynamically adjusting control parameters in real-time [11-13]. By implementing BS, renewable energy systems can optimize power conversion, reduce performance variability, and enhance overall system efficiency, thus addressing the inherent limitations of current renewable energy technologies.

To address these challenges and optimize microgrid performance, advanced control strategies are essential. Traditional control methods, such as Proportional-Integral (PI) controllers, while widely used, often struggle to handle the nonlinear dynamics and uncertainties inherent in microgrid systems, particularly those with high renewable energy penetration. This research focuses on enhancing the performance of a grid-connected microgrid system through the implementation of backstepping (BS) controllers, a nonlinear control technique known for its robustness and adaptability. The study compares three control systems: a conventional system using the Perturb and Observe (P&O) algorithm for Maximum Power Point Tracking (MPPT) and PI controllers for grid-side converter (GSC) control, a hybrid system with BS-modified P&O (BS-P&O) for MPPT and PI controllers for GSC, and an advanced system employing BS-P&O for MPPT and BS controllers for GSC.

The primary objectives of this research are to improve the efficiency of the PV system, enhance the power quality of the microgrid, and optimize the overall system performance under various operating conditions. By implementing BS controllers, the study aims to achieve better regulation of DC-link voltage, more effective management of active and reactive powers, and reduction in Total Harmonic Distortion (THD). The comparative analysis of the three control strategies provides insights into the effectiveness of nonlinear control techniques in microgrid applications. This research contributes to the ongoing efforts to develop more resilient, efficient, and sustainable energy systems, addressing the critical need for advanced control solutions in the context of increasing renewable energy integration and the evolving landscape of smart grid technologies. This research introduces a novel approach by integrating a Backstepping (BS) controller with the Perturb and Observe (P&O) algorithm for Maximum Power Point Tracking (MPPT) in photovoltaic (PV) systems within a microgrid framework. The significance of this work lies in its advanced control strategy, which enhances DC-link voltage regulation through dual-loop control, ensuring better stability and power quality, especially during dynamic environmental changes. The BS controller effectively reduces Total Harmonic Distortion (THD), thereby improving the quality of power exchanged with the grid. Furthermore, the system enables efficient bidirectional power flow, enhancing the flexibility of energy transfer between the microgrid and the main grid. A comprehensive comparative analysis demonstrates that the BS-P&O with BS controllers outperforms traditional control methods in efficiency, dynamic response, and robustness, underscoring the potential of nonlinear control techniques in optimizing microgrid performance and renewable energy integration. Despite its significant improvements, this work is limited by the complexity of implementing Backstepping (BS) controllers, which require precise system modeling and can be computationally intensive. Additionally, the approach's performance may vary under extreme or highly unpredictable environmental conditions, potentially affecting its robustness in real-world applications.

2. LITERATURE REVIEW

The efficiency of photovoltaic (PV) systems is a critical concern in renewable energy research.

Maximum Power Point Tracking (MPPT) is widely recognized as an effective technique for optimizing PV system performance, particularly under varying atmospheric conditions. Various MPPT methods have been proposed in the literature, each addressing specific challenges related to dynamic performance and efficiency. In recent studies, advanced MPPT techniques have been developed to enhance the power output and minimize oscillations around the Global Maximum Power Point (GMPP). For instance, an integration of Grey Wolf Optimization (GWO) with Adaptive Neuro-Fuzzy Inference Systems (ANFIS) was proposed by [14], which effectively fine-tunes power output with minimal oscillations. This method demonstrated precise GMPP tracking and negligible oscillations, which are crucial for maintaining high PV system efficiency. Another significant contribution is the Model Reference Adaptive Control (MRAC) method, compared with conventional techniques like Perturb and Observe (P&O), Incremental Conductance (INC), Particle Swarm Optimization (PSO), and GWO [15]. The MRAC approach showed substantial improvements in tracking efficiency and convergence speed, especially under rapidly changing meteorological conditions. This underscores the method's robustness and effectiveness in real-time PV system management. Enhanced P&O techniques have also been explored to balance the trade-off between steady-state oscillations and dynamic response in MPPT systems. For example, an improved P&O method utilizing the relationship between open-circuit voltage and maximum power voltage was proposed in [16]. This method establishes a confined search space, leading to better stability and performance in real-time simulations. On the grid integration side, after the PV system generates electrical energy, it must be efficiently transmitted to the electrical grid. Voltage-Oriented Control (VOC) has emerged as a prominent strategy in managing this process. Moreover, a control approach for a three-phase system powered by sinusoidal PWM in the stationary reference frame was introduced in [17], utilizing proportional-resonant controllers. This approach was noted for its high dynamic performance, ease of implementation, and effective attenuation of converter switching-related harmonics. Further advancements include the use of Linear Quadratic Regulators (LQR) for Voltage Source Inverters (VSIs) in renewable energy systems [18-19]. LQR-based control strategies have shown success in minimizing Total Harmonic Distortion (THD) and achieving unity power factor (UPF), ensuring high-quality power delivery to the grid even under unbalanced conditions. A novel Direct Power Control (DPC) technique was also introduced in [20] for a grid-connected solar power system. This method effectively manages both instantaneous active and reactive power, optimizing power flow and voltage levels on both the DC and AC sides of the system.

Overall, GWO-ANFIS and MRAC offer superior accuracy, faster convergence, and enhanced adaptability for MPPT in PV systems compared to traditional methods like P&O and INC. However, these advantages come with increased computational complexity, requiring more processing power and memory, which can limit their use in resource-constrained systems. Additionally, their reliance on precise modeling (MRAC) or iterative learning (GWO-ANFIS) increases implementation costs and complexity. In contrast, traditional methods remain more practical for simpler, cost-sensitive applications due to their lower computational demands and ease of deployment.

3. PROBLEM STATEMENTS AND CONTRIBUTIONS

This research addresses critical challenges in microgrid systems integrating renewable energy sources, particularly solar PV, with the main grid. The primary issues include the need for efficient bidirectional power flow, adaptive control under variable environmental conditions, maintenance of power quality, and overall system efficiency improvement. Traditional control methods often fall short of exploiting the full potential of these systems, lacking robustness against disturbances and uncertainties. To address these challenges, this study introduces several key contributions.

Firstly, it proposes an enhanced Maximum Power Point Tracking (MPPT) algorithm by integrating a Backstepping (BS) controller with the conventional Perturb and Observe (P&O) method, termed BS-P&O. This approach aims to improve tracking speed and efficiency under dynamic conditions. Secondly, it implements a comprehensive Backstepping control strategy for the grid-side converter, enhancing DC-link voltage regulation and power management. The research presents a holistic optimization approach by applying Backstepping controllers throughout the microgrid system. Furthermore, it focuses on power quality enhancement, aiming to reduce Total Harmonic Distortion (THD) and achieve near-unity power factor operation. A comparative analysis between traditional, partially improved, and fully optimized control methods provides valuable insights into the incremental benefits of each enhancement. The proposed strategies demonstrate tangible improvements in overall system efficiency and exhibit superior robustness against external disturbances, contributing to more stable and reliable microgrid operation. This comprehensive approach significantly advances microgrid technology, facilitating more efficient and reliable integration of renewable energy sources into the electrical grid.

Traditional methods in microgrid control, such as the conventional Perturb and Observe (P&O) algorithm for Maximum Power Point Tracking (MPPT), often suffer from slow response times, with tracking inefficiencies resulting in energy losses of up to 10-15% under rapidly changing conditions. Grid-side control strategies based on traditional approaches struggle to maintain DC-link voltage stability, especially during transient events, leading to power conversion efficiency losses of up to 8%. Additionally, Total Harmonic Distortion (THD) frequently exceeds the 5% threshold, compromising power quality and grid stability, while achieving near-unity power factor remains a challenge due to inadequate reactive power compensation.

4. METHODOLOGY AND SYSTEM MODELLING

The methodology of this work involves designing and comparing three control systems for a microgrid integrating a photovoltaic (PV) system. First, a traditional control system uses the Perturb and Observe (P&O) algorithm for Maximum Power Point Tracking (MPPT) and Proportional-Integral (PI) controllers for the grid-side converter (GSC). Next, a hybrid system integrates a Backstepping (BS) controller with the P&O algorithm (BS-P&O) for MPPT while retaining PI controllers for GSC. Finally, an advanced system combines BS-P&O for MPPT and BS controllers for GSC. Each control system is evaluated through simulations under varying solar irradiance and battery conditions, focusing on metrics like DC-link voltage regulation, active and reactive power management, and Total Harmonic Distortion (THD) reduction.

Figure 1 depicts the structure of the proposed microgrid system. It illustrates a small DC grid connected to the main power grid. The microgrid consists of a photovoltaic (PV) system and a battery for energy storage.

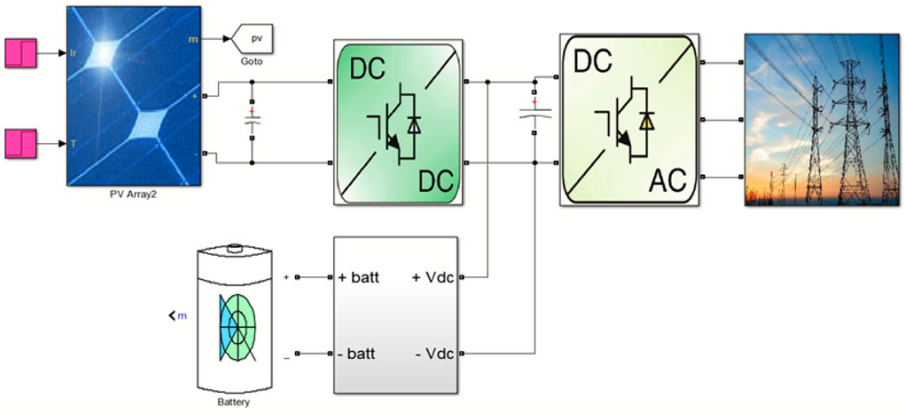

Figure 1. Depiction of the proposed microgrid.

The PV system is connected to a DC-DC boost converter, which is then linked to a DC bus. The battery is also connected to this DC bus. A three-phase inverter (labeled as VSI - Voltage Source Inverter) interfaces the DC bus with the main AC grid through a filter. This configuration allows for bidirectional power flow between the microgrid and the main grid, enabling efficient energy management and integration of renewable resources.

4.1. DC-DC Converter

The structure of a boost converter is illustrated in Figure 2, which is a type of DC-DC power converter. The diagram shows the basic components of the boost converter circuit.
It consists of an inductor (L) connected to the input voltage source (V_s), a power electronic switch (typically a MOSFET or IGBT), a diode, and an output capacitor (C) connected to the load (represented by V_0). The switch is controlled by a duty cycle (D) to regulate the output voltage. This configuration allows the boost converter to produce an output voltage that is higher than its input voltage, hence its name "boost" converter. The boost converter is a key component in the PV system, helping to step up the voltage from the solar panels to the required DC bus voltage level. The dynamic model of the boost chopper is as follows [21, 22].

$$\frac{dI_L}{dt} = \frac{-(1-D)V_o + V_s}{L} \qquad (1)$$

$$\frac{dV_o}{dt} = \frac{(1-D)I_L - I_o}{C} \qquad (2)$$

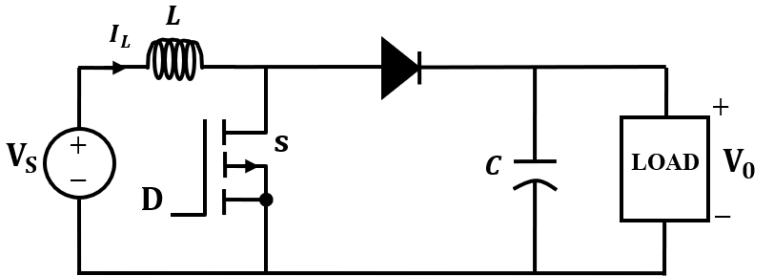

Figure 2. Electrical circuit of the boost converter.

4.2. Grid side converter modeling

The description of the transistor converter, when connected to a balanced three-phase electrical network is based on the following expressions.

$$\begin{cases} V_a = V_m \sin(\omega_s t) \\ V_b = V_m \sin(\omega_s t - \frac{2\pi}{3}) \\ V_c = V_m \sin(\omega_s t + \frac{2\pi}{3}) \end{cases} \qquad (3)$$

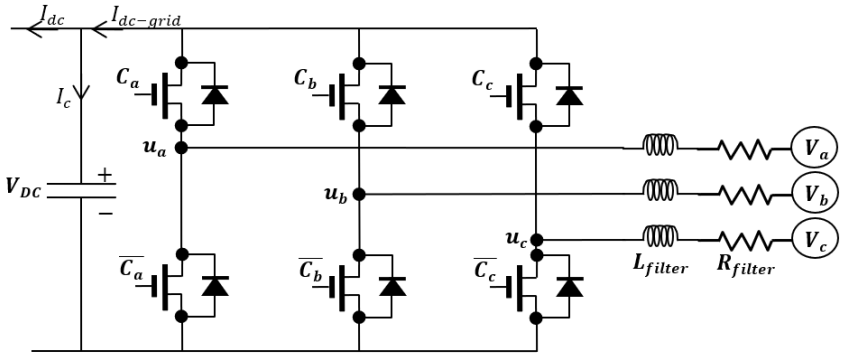

Figure 3. Grid-side converter structure.

The voltage balance equations can expressed as follow.

$$\begin{cases} V_a - u_a = R_{rec} i_a + L_{rec} \dfrac{di_a}{dt} \\ V_b - u_b = R_{rec} i_b + L_{rec} \dfrac{di_b}{dt} \\ V_c - u_c = R_{rec} i_c + L_{rec} \dfrac{di_c}{dt} \end{cases} \qquad (4)$$

In the three columns, the voltages of the transistor converter are determined based on the state of the electronic switches and the value of the intermediate circuit voltage. The following equations can explain this feature.

$$\begin{bmatrix} u_a \\ u_b \\ u_c \end{bmatrix} = \frac{V_{dc}}{3} \begin{bmatrix} 2 & -1 & -1 \\ -1 & 2 & -1 \\ -1 & -1 & 2 \end{bmatrix} \begin{bmatrix} C_a \\ C_b \\ C_c \end{bmatrix} \qquad (5)$$

Eq (6) gives the dc-link voltage

$$\frac{dV_{dc}}{dt} = \frac{1}{C}(i_{dc-grid} - i_{dc}) \qquad (6)$$

The GSC is given in a d-q frame as follow [23-25].

$$V_d = R_{filter} i_d + L_{filter} \frac{di_{d\ filter}}{dt} - \omega_s L_{filter} i_{q\ filter} + u_d \qquad (7)$$

$$V_q = R_{filter} i_q + L_{rec} \frac{di_{q\ filter}}{dt} + \omega_s L_{filter} i_{d\ filter} + u_q \qquad (8)$$

5. CONTROL OBJECTIVES

5.1. Control of DC-DC Converter

To design the MPPT controller, two methods have been used.

1. The first one is the P&O algorithm; its flowchart is shown in Figure 4.
2. The second method aims to improve the performance of the MPPT unit by modifying the output of the P&O algorithm. Instead of the output being the duty cycle (D), it will now be the reference value for the input current of the boost converter (IL). The same flowchart in Figure 4 is maintained with the replacement of D with $I_{L\text{-}ref}$.

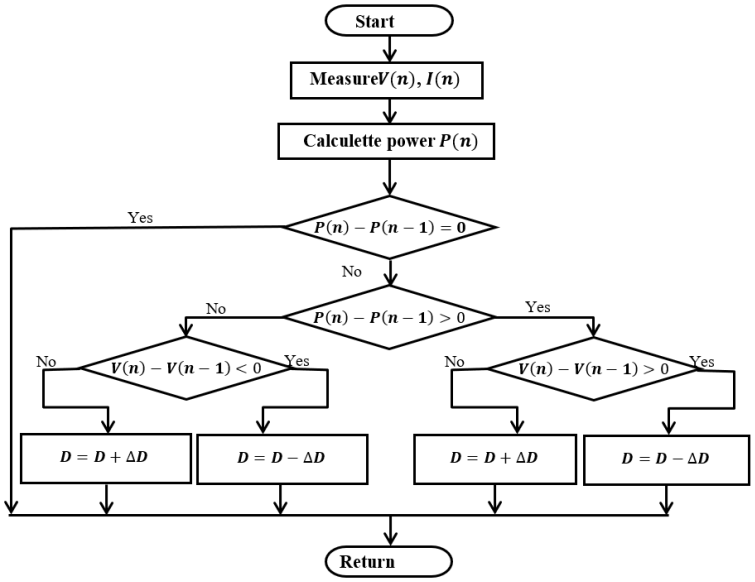

Figure 4. Flowchart of P&O algorithm.

Subsequently, the input current of the dc-dc converter is regulated according to the following relationships.
First suppose,

$$e_L = I_L^* - I_L \qquad (9)$$

The following results from deriving the Eq (9) and inserting the relation (2).

$$\dot{e}_L = \frac{dI_L^*}{dt} + \frac{V_o}{L} - \frac{DV_o}{L} - \frac{V_s}{L} \qquad (10)$$

Assume the following is the Lyapunov function formula.

$$v_L = 0.5c_1 {e_L}^2 + 0.5c_2 {z_L}^2 \qquad (11)$$

Where,

$$z_L = \int e_L \, dt \qquad (12)$$

Following the derivation of relation (11) and substitution of relation (12), the following is obtained.

$$\dot{v}_L = c_1 \dot{e}_L e_L + c_2 z_L e_L \qquad (13)$$

Upon replacing the relation (10), the result is:

$$\dot{v}_L = c_1 e_L \frac{dI_L^*}{dt} + c_1 e_L \frac{V_o}{L} - c_1 e_L \frac{DV_o}{L} - c_1 e_L \frac{V_s}{L} + c_2 z_L e_L \qquad (14)$$

Eq (14) may be solved to yield

$$\dot{v}_L = -k\, {e_L}^2 + e_L \left(c_1 \frac{dI_L^*}{dt} + c_1 \frac{V_o}{L} - c_1 \frac{DV_o}{L} - c_1 \frac{V_s}{L} + c_2 z_L + k\, e_L \right) \qquad (15)$$

The Lyapunov function (v_L) derivative must be negative in order to be:

$$D = \frac{1}{c_1 V_o} \left(c_1 \frac{dI_L^*}{dt} + c_1 \frac{V_o}{L} - c_1 \frac{V_s}{L} + c_2 z_L + k\, e_L \right) \qquad (16)$$

5.2. Control of DC-AC Converter

It is possible to derive the following relations for electrical power, assuming that the rotating

d,qframe is orientated such that the d-axis corresponds with the network voltage vector.

$$P = V_d\, i_d \qquad (17)$$

$$Q = -V_d\, i_q \qquad (18)$$

When the reference value of i_q is set to zero, the relationship for the active power can be expressed as follows, yielding a unit power factor.

$$P = V_d\, i_d = V_{dc}\, i_{dc-grid} \qquad (19)$$

Thus, there are two regulating axes in the GSC control system: the current i_q is controlled at zero on the q-axis and the d-axis has two regulating loops: an internal regulating loop that regulates current i_d, and an external regulating loop that regulates dc-link voltage.

5.2.1. Current controller design

Let's first assume,

$$e_d = i^*_{d\ filter} - i_{d\ filter} \qquad (20)$$

The following results from deriving the Eq (20) and inserting the relation (8).

$$\dot{e}_d = \frac{di^*_{d\ filter}}{dt} + \frac{R_{filter}}{L_{filter}} i_{d\ filter} - \omega_s\, i_{q\ filter} - \frac{V_d}{L_{filter}} + \frac{u_{d\ filter}}{L_{filter}} \qquad (21)$$

Assume the following is the Lyapunov function formula.

$$v_d = 0.5\gamma_1 e_d^{\,2} + 0.5\gamma_2 z_d^{\,2} \qquad (22)$$

Where,

$$z_d = \int e_d\, dt \qquad (23)$$

Following the derivation of relation (22) and substitution of relation (23), the following is obtained.

$$\dot{v}_d = \gamma_1 \dot{e}_d e_d + \gamma_2 z_d e_d \qquad (24)$$

Upon replacing the relation (21), the result is:

$$\dot{v}_d = \gamma_1 \left(\frac{di^*_{d\ filter}}{dt} + \frac{R_{filter}}{L_{filter}} i_{d\ filter} - \omega_s\, i_{q\ filter} - \frac{V_d}{L_{filter}} + \frac{u_{d\ filter}}{L_{filter}} \right) e_d + \gamma_2 z_d e_d \qquad (25)$$

Equation (25) may be solved to yield,

$$\dot{v}_d = -k_1 e_d^{\,2} + e_d \left(\frac{di^*_{d\ filter}}{dt} + \frac{R_{filter}}{L_{filter}} i_{d\ filter} - \omega_s\, i_{q\ filter} - \frac{V_d}{L_{filter}} + \frac{u_{d\ filter}}{L_{filter}} + \frac{\gamma_2}{\gamma_1 z_d} + \frac{k_1}{\gamma_1 e_d} \right) \qquad (26)$$

The Lyapunov function (v_d) derivative must be negative in order to be,

$$u^*_{d\ filter} = L_{filter} \left(-\frac{di^*_{d\ filter}}{dt} + \frac{R_{filter}}{L_{filter}} i_{d\ filter} - \omega_s\, i_{q\ filter} - \frac{V_d}{L_{filter}} + \frac{u_{d\ filter}}{L_{filter}} + \frac{\gamma_2}{\gamma_1 z_d} + \frac{k_1}{\gamma_1 e_d} \right) \qquad (27)$$

Similarly, one can get the following to control the current on the q-axis:

$$u^*_{q\ filter} = L_{filter} \left(-\frac{di^*_{q\ filter}}{dt} + \frac{R_{filter}}{L_{filter}} i_{q\ filter} - \omega_s\, i_{d\ filter} - \frac{V_q}{L_{filter}} + \frac{u_{d\ filter}}{L_{filter}} + \frac{\gamma_4}{\gamma_3 z_q} + \frac{k_2}{\gamma_3 e_q} \right) \qquad (28)$$

Where,

$$e_q = i^*_{q\ filter} - i_{q\ filter} \qquad (29)$$

and,

$$z_q = \int e_q\, dt \qquad (30)$$

It should be noted that c_i, γ_i, k_i are positive constants.
Eq (31) is used to go from the abc frame to the *d,q* frame, and Eq (32) is used to travel from the α,β frame to the *d,q* frame.

$$\begin{bmatrix} X_d \\ X_q \end{bmatrix} = \sqrt{\frac{2}{3}} \begin{bmatrix} cos(\theta) & cos(\theta - \frac{2\pi}{3}) & cos(\theta + \frac{2\pi}{3}) \\ -sin(\theta) & -sin(\theta - \frac{2\pi}{3}) & -sin(\theta + \frac{2\pi}{3}) \end{bmatrix} \begin{bmatrix} X_a \\ X_b \\ X_c \end{bmatrix} \quad (31)$$

$$\begin{bmatrix} X_d \\ X_q \end{bmatrix} = \begin{bmatrix} cos(\theta) & sin(\theta) \\ -sin(\theta) & cos(\theta) \end{bmatrix} \begin{bmatrix} X_\alpha \\ X_\beta \end{bmatrix} \quad (32)$$

5.2.2. Dc Link voltage controller design

Assuming that i_{dc} represents the external disturbance, the relationship (6) becomes.

$$\frac{dV_{dc}}{dt} = \frac{1}{C} i_{dc-grid} \quad (33)$$

Based on the relationship (19), the following can be written,

$$\frac{dV_{dc}}{dt} = \frac{a}{C} i_d \quad (34)$$

Where, $a = \frac{V_d}{V_{dc}}$.

Considering that the equation represents a first-order transfer function with a pole equal to zero, a first regulating loop with a proportional constant will first be added to change the position of the pole, according to the following.
Let's suppose,

$$e_{dc1} = V_{dc1} - V_{dc} \quad (35)$$

By deriving the relationship (35) and after replacing the relationship (34), it becomes as follows.

$$\dot{e}_{dc1} = -\frac{a}{c} i_d \quad (36)$$

Now, the Lyapunov function is imposed according to the following formula.

$$v_{dc1} = 0.5 \gamma_5 {e_{dc1}}^2 \quad (37)$$

By differentiating the relationship (37), it be founded.

$$\dot{v}_{dc1} = \gamma_5 \dot{e}_{dc1} e_{dc1} \quad (38)$$

By substituting the relationship (36), it becomes as:

$$\dot{v}_{dc1} = \gamma_5 \left(-\frac{a}{c} i_d \right) e_{dc1} \quad (39)$$

From Eq (39), it becomes as:

$$\dot{v}_{dc1} = -e_{dc1}^2 + e_{dc1} \left(e_{dc1} + \gamma_5 \left(-\frac{a}{c} i_d \right) \right) \quad (40)$$

The reference current on the d-axis can be obtained, as shown.

$$i_{d\ ref} = \frac{C}{\gamma_5\ a} (e_{dc1}) \quad (41)$$

Therefore, the transfer function of the internal voltage regulator loop will have equal pole $1/\gamma_5$.

The differential equation linking V_{dc} and V_{dc1} becomes as follows.

$$\frac{dV_{dc}}{dt} = \frac{1}{\gamma_5} V_{dc1} - \frac{1}{\gamma_5} V_{dc} \qquad (42)$$

To obtain accurate voltage regulation and overcome external disturbances, a second regulation loop is added according to the following steps.

$$e_{dc} = V_{dc-ref} - V_{dc} \qquad (43)$$

By deriving and after replacing the relationship (42), the relationship (43) becomes as:

$$\dot{e}_{dc} = \frac{1}{\gamma_5} V_{dc1} - \frac{1}{\gamma_5} V_{dc} \qquad (44)$$

The Lyapunov function is imposed according to the following formula.

$$v_{dc} = 0.5\gamma_6 {e_{dc}}^2 + 0.5\gamma_7 {z_{dc}}^2 \qquad (45)$$

Where,

$$z_{dc} = \int e_{dc}\, dt \qquad (46)$$

By differentiating the relationship (45) and substituting the relationship (46), it becomes.

$$\dot{v}_{dc} = \gamma_6 \dot{e}_{dc} e_{dc} + \gamma_7 z_{dc} e_{dc} \qquad (47)$$

By substituting the relationship (44), relation (45) becomes.

$$\dot{v}_{dc} = \gamma_6 \left(\frac{1}{\gamma_5} V_{dc1} + \frac{1}{\gamma_5} V_{dc} \right) e_{dc} + \gamma_7 z_{dc} e_{dc} \qquad (48)$$

By fixing Eq (49), Eq (50) can be obtained as:

$$\dot{v}_{dc} = -k_3 {e_{dc}}^2 + e_{dc} \left(-\frac{\gamma_6}{\gamma_5} V_{dc1} + \frac{\gamma_6}{\gamma_5} V_{dc} + \gamma_7 z_{dc} \right) \qquad (49)$$

To make Lyapunov function derivative in Eq (49) negative, it must be:

$$v_{dc1} = \frac{\gamma_5}{\gamma_6} \left(\frac{\gamma_6}{\gamma_5} V_{dc} + \gamma_7 z_{dc} + k_3 e_{dc} \right) \qquad (50)$$

6. SIMULATION RESULTS, ANALYSIS AND DISCUSSION

In this section, the performance of the control system is discussed. The system parameter values are shown in appendix A.

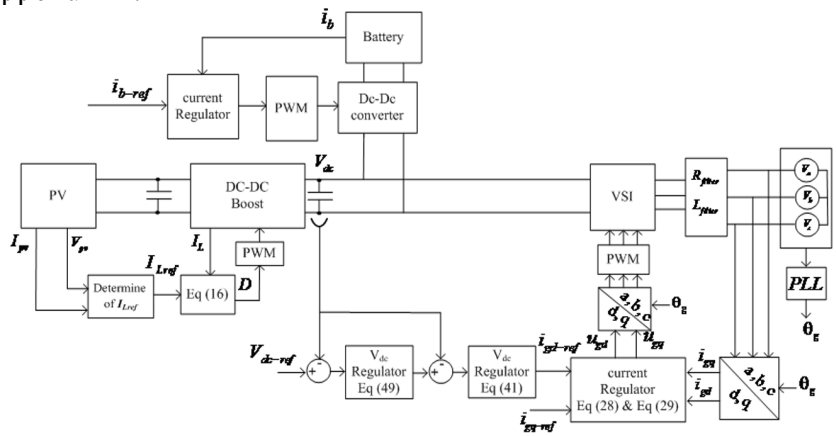

Figure 5. Control system diagram for the proposed microgrid.

A comparison was made between three control systems:
1. The first system includes traditional methods, in which a P&O algorithm in the MPPT system and PI controller of GSC.
2. The second control system includes BS controller based modified P&O algorithm (BS-P&O) in the MPPT system, and PI controller of GSC.
3. The third control system includes BS-P&O in the MPPT system, and BS controller of GSC, so the control system diagram becomes as shown in the Figure 5.

The solar radiation profile (with the temperature held constant at 25°C) used in the simulation study is illustrated in Figure 6. The graph shows the variation of solar irradiance over time, with three distinct levels of radiation intensity. The profile starts at a moderate level of 800 W/m², which is maintained for a period before suddenly increasing to 1000 W/m². This higher level of irradiance is sustained for some time, representing optimal solar conditions. Finally, the profile experiences another abrupt change, dropping back to 800 W/m². This step-wise pattern in solar radiation allows the researchers to evaluate the performance of different control systems under varying solar input conditions, simulating real-world scenarios where solar intensity can change rapidly due to factors like cloud cover or time of day.

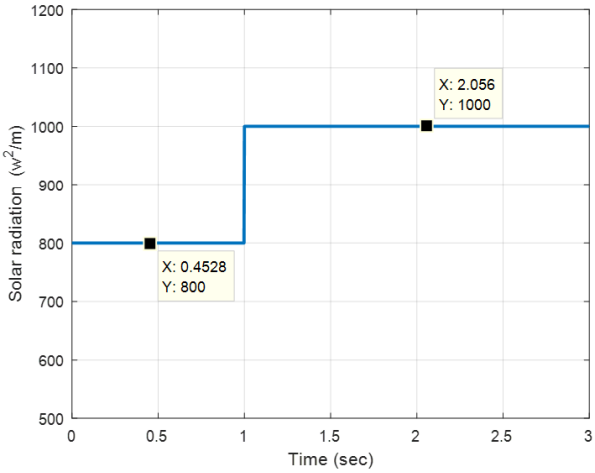

Figure 6. Solar radiation profile.

The battery charging/discharging current is shown in the Figure 7. The graph shows a step-wise mode of battery current over time, illustrating how the battery alternates between charging and discharging modes. Initially, the battery current is at 10 A, indicating a discharging state where the battery is supplying energy to the system. This discharging phase continues for a period before abruptly switching to a charging state, represented by a current of -10 A. The negative value signifies that the battery is now storing excess power from the system. This alternating mode between charging and discharging continues throughout the simulation, with sharp transitions between the two states. Such a profile allows researchers to evaluate how the control systems handle sudden changes in energy flow direction and magnitude, simulating real-world scenarios where energy storage systems must quickly respond to varying supply and demand conditions in a microgrid. These sudden changes highlight the system's ability to handle dynamic energy flows, crucial in microgrid environments where supply and demand can vary rapidly. Effective control of these transitions is essential for maintaining system stability, as it ensures that the energy storage system can quickly adapt without causing voltage fluctuations, power losses, or instability in the overall grid.

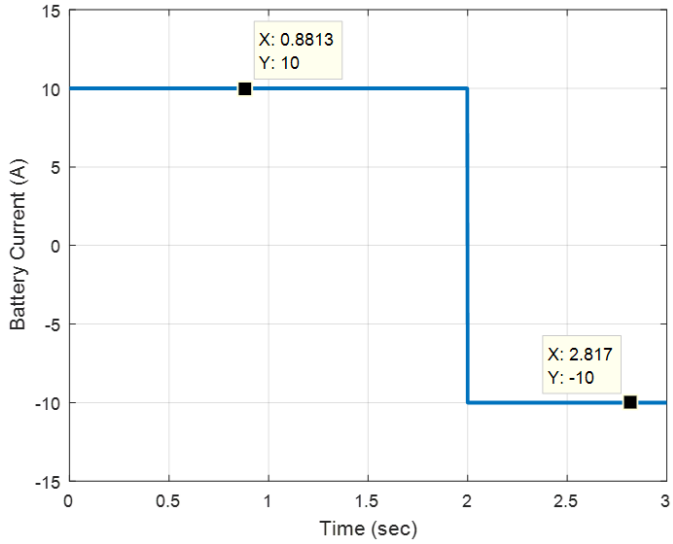

Figure 7. The battery charging/discharging current.

Figure 8 shows the extracted power from the photovoltaic (PV) system under different control strategies. The graph compares three distinct control approaches: a traditional P&O (Perturb and Observe) algorithm with PI (Proportional-Integral) controllers, a modified BS-P&O (Backstepping-P&O) algorithm with PI controllers, and a BS-P&O algorithm with BS controllers.

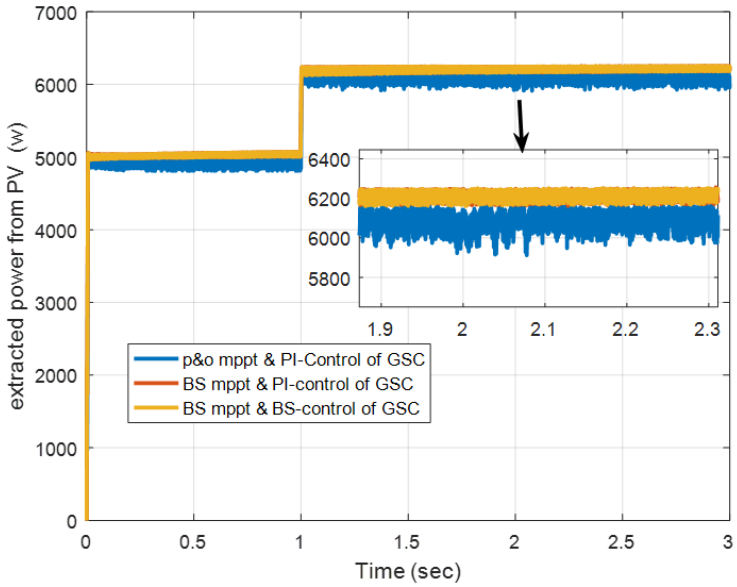

Figure 8. The extracted power from the PV system under different control strategies.

The power output closely follows the solar radiation profile shown in Figure 6, demonstrating the direct relationship between solar irradiance and PV power generation. Initially, when the solar radiation is at 800 W/m², all three control strategies extract similar amounts of power, around 5000W. However, as the solar radiation increases to 1000 W/m², the power output rises accordingly, reaching approximately 6400W. During this period of higher irradiance, the BS-P&O methods (both with PI and BS controllers) show slightly superior performance, extracting marginally more power than the traditional P&O method. This difference becomes more pronounced when the solar radiation drops back to 800 W/m², where the BS-P&O strategies maintain a higher power output compared to the conventional P&O approach. The graph demonstrates the enhanced efficiency of the BS-P&O methods in maximizing power extraction

from the PV system, particularly during changes in solar irradiance.

Figure 9 presents the efficiency curves of the MPPT controllers under different control strategies. The graph compares the efficiency of three approaches: traditional P&O algorithm with PI controllers, BS-P&O with PI controllers, and BS-P&O with BS controllers. The efficiency is plotted over time, corresponding to the changing solar radiation profile shown in Figure 6. Initially, when the solar radiation is at 800 W/m², all three strategies show relatively high efficiency, but the BS-P&O methods (both with PI and BS controllers) demonstrate slightly higher efficiency than the traditional P&O approach. As the solar radiation increases to 1000 W/m², there's a momentary dip in efficiency for all strategies, likely due to the rapid change in conditions. However, the BS-P&O methods recover more quickly and maintain higher efficiency during this period of increased irradiance. The superiority of the BS-P&O strategies becomes even more evident when the solar radiation drops back to 800 W/m². During this transition, the BS-P&O methods, especially the one with BS controllers, maintain significantly higher efficiency compared to the conventional P&O approach. Throughout the simulation, the BS-P&O with BS controllers consistently shows the highest efficiency, followed closely by BS-P&O with PI controllers, while the traditional P&O method lags. This graph clearly illustrates the enhanced performance of the backstepping-based MPPT strategies in maintaining high efficiency across varying solar conditions.

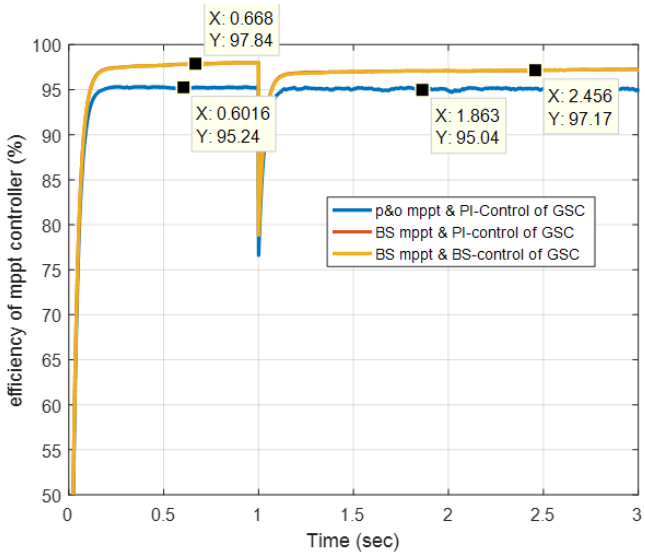

Figure 9. Efficiency feature of the MPPT controllers.

Figure 10 illustrates the response of different control systems in regulating the DC-link voltage. From this figure, a comparison of three control strategies is conducted: traditional P&O with PI controllers, BS-P&O with PI controllers, and BS-P&O with BS controllers. The DC-link voltage is plotted over time, with the reference voltage set at 600V. All three systems start at the same initial voltage and attempt to reach and maintain the reference value. The BS-P&O with BS controllers achieves the reference voltage rapidly (600V within 0.05 to 0.5 seconds) and exhibits minimal oscillations (<1 to 2%), reflecting its superior stability. The BS-P&O with PI controllers shows the second-best performance, with a slightly slower response time and marginally more oscillation than the BS-BS system. The traditional P&O with PI controllers exhibits the slowest response and the most significant oscillations around the reference voltage. Notably, all systems experience some disturbances, likely corresponding to changes in solar radiation or battery current, but the BS-BS system shows superior ability in quickly overcoming these disturbances and returning to the reference voltage. This graph clearly illustrates the enhanced dynamic performance and disturbance rejection capabilities of the backstepping-based control strategies, particularly the BS-P&O with BS controllers, in maintaining a stable DC-link voltage under varying conditions.

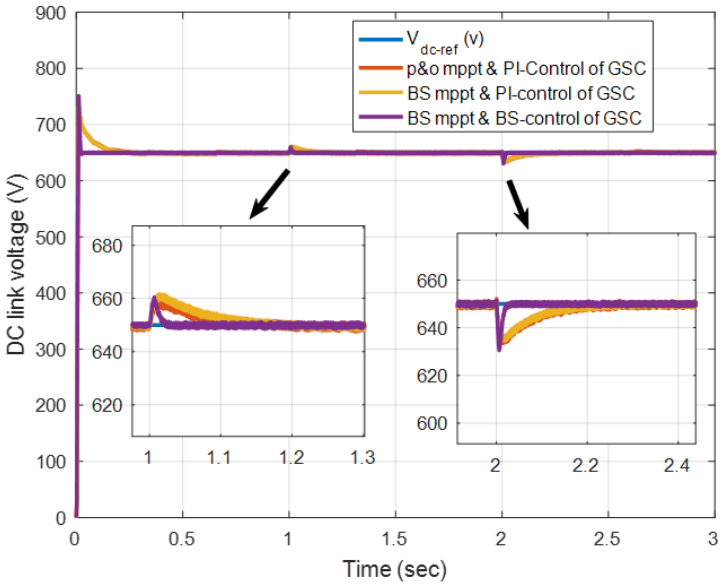

Figure 10. Control systems response to regulate the dc-link voltage.

The active power transmitted to the grid under different control systems is illustrated in Figure 11. The characteristic shows three distinct curves representing the performance of various control strategies. The blue curve, corresponding to the traditional P&O algorithm with PI controllers, demonstrates the lowest active power transmission to the grid. The red curve, representing the BS-P&O controller with PI controllers for the grid-side converter, shows an improvement in active power transmission compared to the traditional method. However, the green curve, which depicts the performance of the BS-P&O controller combined with BS controllers for the grid-side converter, clearly outperforms the other two methods. This third control system achieves the highest active power transmission to the grid, indicating superior efficiency and utilization of the available power. The graph also reveals that all three control systems respond to changes in solar radiation and battery current, as evidenced by the variations in active power output over time. The superior performance of the BS controllers in maximizing power transfer to the grid underscores their effectiveness in optimizing microgrid operations and enhancing overall system efficiency.

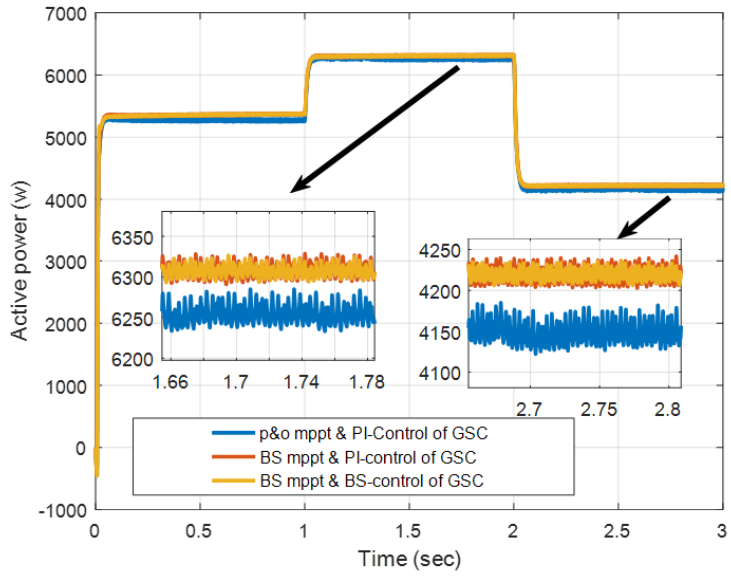

Figure11. Active power transmitted to the grid.

The reactive power exchanged with the grid for the three different control systems studied in this research is represented Figure 12. This figure illustrates the performance of each control strategy in managing reactive power, which is crucial for maintaining grid stability and power quality. The blue curve represents the traditional P&O algorithm with PI controllers, showing the largest fluctuations in reactive power exchange. This indicates that this control system struggles to maintain a consistent reactive power close to zero, which is generally desired for optimal grid interaction. The red curve, depicting the BS-P&O controller with PI controllers for the grid-side converter, demonstrates an improvement over the traditional method, with reduced reactive power fluctuations.

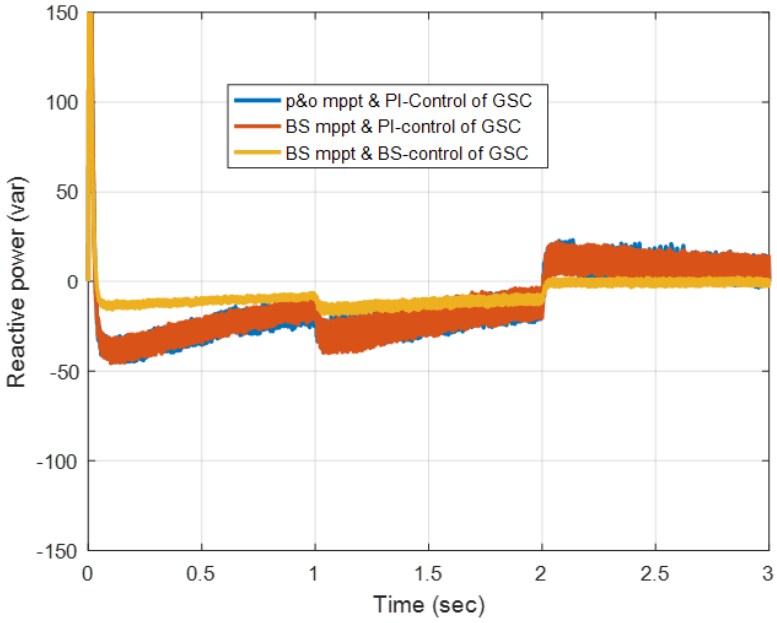

Figure 12. Reactive power exchanged with grid.

However, the green curve, representing the BS-P&O controller combined with BS controllers for the grid-side converter, exhibits the best performance among the three systems. This advanced control strategy maintains the reactive power closest to zero throughout the simulation, with minimal deviations. The superior performance of the BS controllers in managing reactive power exchange highlights their ability to enhance power factor correction and improve overall grid integration. The graph also shows that all three control systems respond to changes in operating conditions, such as variations in solar radiation and battery current, but the BS controllers demonstrate the most robust and stable response in maintaining near-zero reactive power exchange with the grid.

Figure 13 illustrates the Total Harmonic Distortion (THD) curve of the current exchanged with the grid under different control scenarios. The results reveal that the use of Backstepping (BS) controllers, either combined with the Perturb and Observe (P&O) algorithm or in conjunction with another BS controller, leads to significantly lower THD values compared to traditional Proportional-Integral (PI) controllers. Specifically, the BS controller achieves the lowest THD, demonstrating its effectiveness in minimizing harmonic distortions and thus enhancing the quality of power transmission. This superior performance is particularly evident when compared to the PI-controlled system, which exhibits higher THD values, indicating more significant distortions. The figure underscores the importance of using advanced control strategies like BS to achieve cleaner and more efficient power exchange with the grid, ultimately leading to improved overall system stability and efficiency.

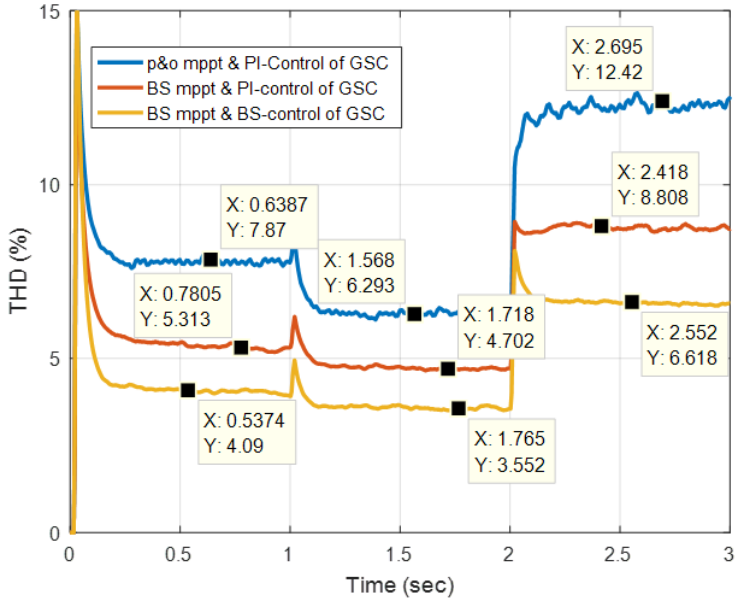

Figure 13. THD feature of the current exchanged with the grid.

Figure 14 presents the FFT analysis of the current exchanged with the grid when Backstepping (BS) controllers are employed. The analysis demonstrates a significant reduction in harmonic components across the frequency spectrum, confirming the effectiveness of BS controllers in minimizing distortion. Unlike conventional Proportional-Integral (PI) controllers, which exhibit noticeable harmonic peaks, the BS controllers maintain a cleaner current waveform, closer to the ideal sinusoidal shape. This improvement in harmonic suppression is crucial for enhancing the power quality and ensuring stable grid operation.

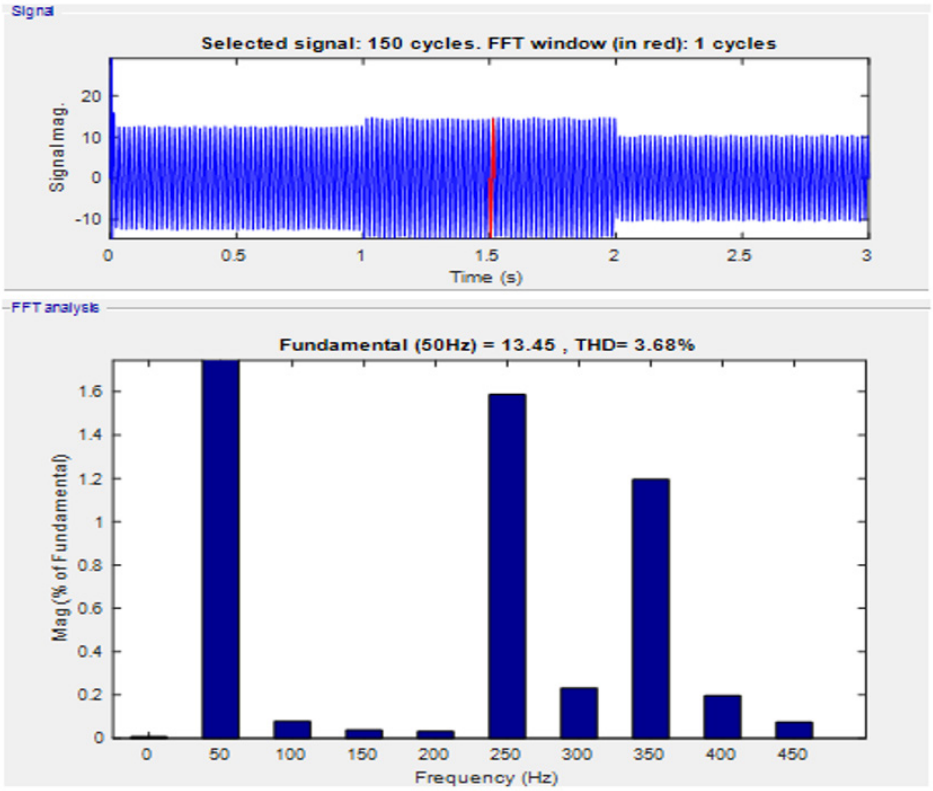

Figure 14. FFT analysis of the current when BS controllers are used.

The FFT results further validate that BS controllers effectively limit the presence of higher-order harmonics, contributing to a lower Total Harmonic Distortion (THD) value. This reduction in THD, as seen in previous figures, is essential for optimizing the efficiency and reliability of the power system, especially in scenarios involving renewable energy integration where power quality is paramount.

The controller's superiority in maintaining grid stability lies in its ability to seamlessly manage rapid transitions between battery charging and discharging states. By effectively regulating the battery current, the controller mitigates voltage fluctuations and ensures a balanced energy flow, even during sudden demand or supply changes. This dynamic response capability enhances system resilience, minimizes power losses, and ensures the grid remains stable under varying operational conditions.

Table 1 compares the efficiency of three control systems under different irradiance and battery current conditions. The first system, which uses a P&O algorithm and PI controllers, shows efficiency ranging from 77% to 96.5%. The second system, integrating a BS-P&O controller with PI controllers, improves efficiency slightly, achieving up to 97.5%. The third system, which combines BS-P&O with BS controllers, maintains the same high efficiency as the second system across all scenarios. This consistency highlights the effectiveness of using BS controllers in enhancing the overall performance of the microgrid system, particularly under varying environmental conditions.

Table 1. Efficiency Comparison of Control Systems under Varying Irradiance and Battery Current Conditions.

control system		**Scenario**		
MPPT controller	control of GSC	I_r=800w²/m I_b=10A	I_r=1000w²/m I_b=10A	I_r=1000w²/m I_b=10A
P&O	PI	95.26 %	95.2 %	95.2 %
BS-P&O	PI	97.85 %	97.12 %	97.12 %
BS-P&O	BS	97.85 %	97.12 %	97.12 %

Table 2 provides a comparison of Total Harmonic Distortion (THD) values for different control systems under various operating conditions. The results show that the traditional system using a P&O algorithm with PI controllers produces the highest THD, particularly under higher irradiance conditions. In contrast, integrating a Backstepping-P&O (BS-P&O) controller with PI controllers reduces the THD, demonstrating an improvement in power quality. The most significant reduction in THD is observed when both the Maximum Power Point Tracking (MPPT) and Grid Side Converter (GSC) are controlled using Backstepping controllers, achieving the lowest THD values across all scenarios. This indicates that Backstepping controllers are highly effective in minimizing harmonic distortions, leading to a more stable and efficient microgrid operation.

Table 2. THD Comparison of Control Systems across Different Operating Scenarios.

control system		**Scenario**		
MPPT controller	control of GSC	I_r=800w²/m I_b=10A	I_r=1000w²/m I_b=10A	I_r=1000w²/m I_b=10A
P&O	PI	7.87 %	6.3 %	12 %
BS-P&O	PI	5.3 %	4.7 %	8.8 %
BS-P&O	BS	4.1 %	3.65 %	6.6 %

Compared to other advanced control strategies in the literature, such as Model Reference Adaptive

Control (MRAC), Incremental Conductance (INC), and Particle Swarm Optimization (PSO)-the BS-based approach in this study demonstrates superior adaptability, faster tracking speed, and better disturbance rejection. For instance, MRAC excels in adaptive conditions but requires extensive computational resources, while PSO-based systems can be slower in convergence. By contrast, BS controllers balance computational efficiency with high dynamic performance, making them a practical and robust solution for real-world microgrid applications. These findings underline the BS controller's potential to enhance the efficiency and resilience of renewable energy systems integrated into modern smart grids. The practical implications of these findings highlight that the BS-P&O with BS controllers significantly improves system efficiency, power quality, and stability, making it particularly suited for real-world applications in smart grids and renewable energy integration. This approach enhances the resilience of microgrids, ensuring optimal performance even in the face of dynamic environmental variations, which is crucial for advancing the deployment of sustainable energy solutions.

7. CONCLUSIONS

This research focused on enhancing the performance of a microgrid system connected to the main grid through a three-phase converter controlled based on Voltage Oriented Control (VOC) method. The microgrid comprised a storage element and a photovoltaic (PV) generation system. The study compared three control systems: 1) a traditional system using a P&O algorithm for MPPT and PI controllers for grid-side converter (GSC), 2) a system with backstepping-based modified P&O (BS-P&O) for MPPT and PI controllers for GSC, and 3) a system employing BS-P&O for MPPT and backstepping controllers for GSC. The results demonstrated that the BS controllers exhibited superior dynamic performance, achieving lower Total Harmonic Distortion (THD) values and contributing to increased efficiency of the microgrid system. Specifically, the third control system, utilizing BS-P&O for MPPT and backstepping controllers for GSC, showed the best performance in terms of tracking speed, overcoming external disturbances, and regulating DC-link voltage, active power, and reactive power. This system achieved the highest efficiency (97.8%) and the lowest THD values (3.66%) among the three systems tested. The research highlights the importance of advanced control techniques in improving the overall performance of grid-connected microgrid systems, particularly in terms of power quality, efficiency, and stability under varying environmental and load conditions.

Future work for this research could expand in several directions. The integration of advanced machine learning algorithms, such as reinforcement learning or neural networks, could further enhance MPPT and grid-side control strategies, potentially leading to even greater efficiency gains. Investigating the system's performance under more complex scenarios with multiple distributed energy sources and varying load profiles would provide insights into its scalability and robustness. Developing adaptive control mechanisms could improve the system's resilience against grid faults and extreme weather conditions, enhancing overall reliability. Real-world implementation and long-term performance analysis would be crucial to validate the simulation results and assess the system's practicality in actual operating conditions. Finally, incorporating sophisticated energy management strategies could optimize the utilization of the battery storage system, potentially leading to improved overall system performance and economic benefits. Moreover, Reinforcement learning (RL) can optimize Maximum Power Point Tracking (MPPT) by continuously learning and adapting to varying environmental conditions such as irradiance and temperature. Establishing a baseline for Total Harmonic Distortion (THD) and efficiency metrics provides a reference to quantify the performance gains achieved through RL, highlighting improvements in energy harvesting and power quality.

Scalability is another important area for future research. The proposed control system

should be tested in larger microgrid configurations or interconnected microgrids to evaluate its robustness and efficiency under more complex operational conditions. Investigating hybrid control approaches that combine BS with other adaptive methods, such as Model Predictive Control (MPC) or Artificial Neural Networks (ANNs), may further improve scalability and resilience. Finally, experimental validation in real-world microgrid environments would provide valuable insights into the system's practical feasibility, especially in terms of hardware integration, communication delays, and fault tolerance in grid-tied and off-grid scenarios.

Authors contribution: Conceptualization M. A. A., B. A., and M. S; methodology, M. A. A., B. A., M. S., B. M., M. B., and S. A. M. M; validation, B.A., B.M., M. B, and S. A. M. M; formal analysis, M. A. A., B. A., M. S., B. M., M. B., and S. A. M. M; resources, all authors; data Curation, all authors; writing—original draft preparation, all authors; writing—review and editing, M. A. A., B.A., and M.B.; All authors have read and agreed to the published version of the manuscript.

Funding: This research received no external funding.

Data Availability Statement: Not applicable.

Conflicts of Interest: The authors declare that they have no known conflicts of interest.

Acknowledgements: This work was supported by the General Directorate of Scientific Research and Technological Development (DGRSDT), the body affiliated to the Algerian Ministry of Higher Education and Scientific Research.

REFERENCES

[1] D. Emara, M. Ezzat, A. Y. Abdelaziz, K. Mahmoud, M. Lehtonen, M. M. Darwish, Novel control strategy for enhancing microgrid operation connected to photovoltaic generation and energy storage systems, Electronics. 10 (2021)1261,https://doi.org/10.3390/electronics10111261.

[2] A. A. Shah, X. Han, H. Armghan, A. A. Almani, A nonlinear integral backstepping controller to regulate the voltage and frequency of an islanded microgrid inverter, Electronics. 10 (2021) 660, https://doi.org/10.3390/electronics10060660.

[3] T. K. Roy, M. A. H. Pramanik, S. K. Ghosh, Design of an integral terminal-based sliding mode controller for PV and BESS-based DC microgrids, Energy Nexus. 7(2022)100130, https://doi.org/10.1016/j.nexus.2022.100130.

[4] H. M. Mehdi, M. K. Azeem, I. Ahmad, Artificial intelligence based nonlinear control of hybrid DC microgrid for dynamic stability and bidirectional power flow, Journal of Energy Storage. 58 (2023) 106333, https://doi.org/10.1016/j.est.2022.106333.

[5] Y. Sahri, S. Tamalouzt, S. L. Belaid, M. Bajaj, S. S. Ghoneim, H. M. Zawbaa, S. Kamel, Performance improvement of hybrid system based DFIG-wind/PV/batteries connected to DC and AC grid by applying intelligent control, Energy Reports. 9 (2023) 2027-2043, https://doi.org/10.1016/j.egyr.2023.01.021.

[6] P. Singh, J. S. Lather, Power management and control of a grid-independent DC microgrid with hybrid energy storage system, Sustainable Energy Technologies and Assessments. 43 (2021)100924, https://doi.org/10.1016/j.seta.2020.100924.

[7] A. S. Mahdi, A. K. Mahamad, S. Saon, T. Tuwoso, H. Elmunsyah, S. W. Mudjanarko, Maximum power point tracking using perturb and observe, fuzzy logic and ANFIS, SN Applied Sciences. 2 (2020)1-9, https://doi.org/10.1007/s42452-019-1886-1.

[8] M. A. Abdourraziq, M. Ouassaid, M., Maaroufi, S. Abdourraziq, Modified P&O MPPT technique for photovoltaic systems. In 2013 International conference on renewable energy research and applications (ICRERA) (2013)(pp. 728-733).

[9] I. Aboudrar, S. El Hani, M. S. Heyine, M. N. Naseri, Dynamic modeling and robust control by ADRC of grid-connected hybrid PV-wind energy conversion system, Mathematical Problems in Engineering. (2019)1-19, https://doi.org/10.1155/2019/8362921.

[10] H. Armghan, M. Yang, A. Armghan, N., Ali, M. O. Wang, I. Ahmad, Design of integral terminal sliding mode controller for the hybrid AC/DC microgrids involving Renewables and energy storage systems, International Journal of Electrical Power & Energy Systems. 119 (2020) 105857, https://doi.org/10.1016/j.ijepes.2020.105857.

[11] A. Taouni, A. Abbou, M. Akherraz, A. Ouchatti, R. Majdoul, MPPT design for photovoltaic system using backstepping control with boost converter, In 2016 International Renewable and Sustainable Energy Conference (IRSEC) (2016) (pp. 469-475). IEEE.

[12] N. Priyadarshi, S. Padmanaban, M. S. Bhaskar, F. Blaabjerg, J. B. Holm-Nielsen, An improved hybrid PV-wind power system with MPPT for water pumping applications, International Transactions on Electrical Energy Systems. 30(2020), e12210, https://doi.org/10.1002/2050-7038.12210.

[13] C. G. Villegas-Mier, J. Rodriguez-Resendiz, J. M. Álvarez-Alvarado, H. Rodriguez-Resendiz, A. M. Herrera-Navarro, O. Rodríguez-Abreo, Artificial neural networks in MPPT algorithms for optimization of photovoltaic power systems: A review, Micromachines. 12(2021), 1260,https://doi.org/10.3390/mi12101260.

[14] R. Ragul, N. Shanmugasundaram, M. Paramasivam, S. Seetharaman, S. L. Mary Immaculate, PV Based Standalone DC-Micro Grid System for EV Charging Station with New GWO-ANFIS MPPTs under Partial Shading Conditions, International Transactions on Electrical Energy Systems. (2023), https://doi.org/10.1155/2023/2073742.

[15] Y. A. Mindzie, J. Kenfack, V. Joseph, U. Nzotcha, D. M. Djanssou, R. Mbounguen, Dynamic performance improvement using model reference adaptive control of photovoltaic systems under fast-changing atmospheric conditions, International Journal of Photoenergy. (2023), https://doi.org/10.1155/2023/5703727.

[16] A. Harrison, E. M. Nfah, J. de Dieu Nguimfack Ndongmo, N. H. Alombah, An enhanced P&O MPPT algorithm for PV systems with fast dynamic and steady-state response under real irradiance and temperature conditions, International Journal of Photoenergy. (2022), https://doi.org/10.1155/2022/6009632.

[17] M. A. Rocha, W. G. De Souza, P. J. A. Serni, A. L. Andreoli, G. A. M. Clerice, P. S. Da Silva, Control of three-phase PWM boost rectifiers using proportional-resonant controllers, In 2018 Simposio Brasileiro de Sistemas Eletricos (SBSE) (2018) (pp. 1-6). IEEE.

[18] V. Rajakumar, K. Anbukumar, I. Selwynraj Arunodayaraj, Power quality enhancement using linear quadratic regulator based current-controlled voltage source inverter for the grid integrated renewable energy system, Electric Power Components and Systems. 45(2017) 1783-1794, https://doi.org/10.1080/15325008.2017.1378773.

[19] S. Sukumaran, E. Arivukkannu, S. P. Thankappan, R. Muthiah, Design of Linear Quadratic Regulator Based Controller for Hybrid Solar-Wind Driven Micro-Grid Inverter, Journal of Green Engineering. 10 (2020) 5380-5400.

[20] H. Tiwari, A. Ghosh, P. K. Ray, B. Subudhi, G. Putrus, M. Marzband, Direct Power Control of a Three-phase AC-DC Converter for Grid-connected Solar Photovoltaic System, In 2021 International Symposium of Asian Control Association on Intelligent Robotics and Industrial Automation (IRIA) (2021) (pp. 125-130). IEEE.

[21] Y. Atifi, A. Raihani, M. Kissaoui, R. Lajouad, K Errakkas, Nonlinear control of three level NPC inverter used in PV/grid system: comparison of topologies and control methods, Bulletin of Electrical Engineering and Informatics. 13 (2024) 2165-2174, https://doi.org/10.11591/eei.v13i3.7122.

[22] S. Marhraoui, A. Abbou, Z. Cabrane, S. E. Rhaili, N. El Hichami, Fuzzy Logic-Integral Backstepping Control for PV Grid-Connected System with Energy Storage Management, International Journal of Intelligent Engineering & Systems.13 (2020), https://doi.org/10.22266/ijies2020.0630.33.

[23] S. Marhraoui, A. Abbou, Z. Cabrane, S. E. Rhaili, N. El Hichami, Fuzzy Logic-Integral Backstepping Control for PV Grid-Connected System with Energy Storage Management, International Journal of Intelligent Engineering & Systems. 13 (2020), https://doi.org/10.22266/ijies2020.0630.33.

[24] I. Aboudrar, S. El Hani, H. Mediouni, A. Aghmad, M. S. Heyine, Robust control of three phase grid connected PV system based on ADRC and fuzzy. In 2018 6th International Renewable and Sustainable Energy Conference (IRSEC) (2018) (pp. 1-6). IEEE.

[25] Y. Atifi, M. Kissaoui, A. Raihani, K. Errakkas, A. Khayat, Advanced Nonlinear Control of WEC System in AC Microgrid Connected to the Main grid With Electric Vehicle Integration, e-Prime-Advances in Electrical Engineering, Electronics and Energy. (2024) 100718, https://doi.org/10.1016/j.prime.2024.100718.

APPENDIX A:

The system parameter values.

Table 3. Photovoltaic Panel Configuration and Specifications.

Parallel strings	3
Series-connected modules per string	10
Maximum Power (W)	213.15
Open circuit voltage Voc (V)	36.3
Voltage at MPPVmp (V)	29
Short-circuit current Isc (A)	7.84
Current at MPP Imp (A)	7.35

Table 4. Grid Characteristics and Parameters.

Parameter	**Value**
R_{filter}	3 Ω
L_{filter}	0.022 H
V_g	220 v
F_g	50Hz

Table 5. Battery Specifications and Parameters.

Parameter	**Value**
Nominal voltage	120v
Rated capacity	240A
Fully charged voltage	139.6v
Nominal discharge current	104.3A